

Efficient and Robust Modeling of Nonlinear Mechanical Systems

Davide Tebaldi[✉], Roberto Zanasi[✉]

University of Modena and Reggio Emilia, Via Pietro Vivarelli 10 - int. 1, Modena, 41125, Italy

Abstract

The development of efficient and robust dynamic models is fundamental in the field of systems and control engineering. In this paper, a new formulation for the dynamic model of nonlinear mechanical systems, that can be applied to different automotive and robotic case studies, is proposed, together with a modeling procedure allowing to automatically obtain the model formulation. Compared with the Euler-Lagrange formulation, the proposed model is shown to give superior performances in terms of robustness against measurement noise for systems exhibiting dependence on some external variables, as well as in terms of execution time when computing the inverse dynamics of the system.

Keywords: Dynamic Modeling, Model Formulation, Physical Systems, Mechanical Systems.

1. Introduction

The development of approaches to model physical systems in different energetic domains has been the subject of studies by many renowned scientists throughout history [1]. Indeed, the dynamic modeling of physical systems is fundamental to develop effective control strategies [2].

The choice of the adopted modeling approach historically depends on the systems energetic domains. When dealing with mechanical systems, the Lagrange equations [3] represent one of the most widespread approaches to derive the dynamic model of the system. Alternatives to the Lagrangian approach involve the initial definition of an augmented dynamic model of the system [4], followed by a model-order reduction assuming rigid connections. As far as electromechanical systems such as electric machines are concerned, they are typically modeled by directly writing the model equations in the desired reference frame [5, 6].

In the context of automotive systems, the detailed modeling of the physical systems involved in a large variety of vehicles, such as planetary gear sets [7], permanent magnet synchronous motors [8] or Full Toroidal Variators (FTVs) [9], represents an important aspect for developing effective energy management strategies [10]. This aspect is strictly related to the calculation of the system inverse dynamics, which allows to compute the optimal actuator torques for energy recovery or trajectory tracking in articulated vehicles. The inverse dynamics problem is also relevant in other areas of engineering, such as robotics for example, where the inverse dynamics control [11] represents the basis for more articulated control approaches such as impedance control [12] or admittance control [13].

The modeling problem becomes more complex when multi-physics systems are considered [14], that are systems composed of physical elements belonging to different energetic domains. In this context, approaches such as Bond Graph (BG) [15, 16], Power-Oriented Graphs (POG) [17, 4], and Energetic Macroscopic Representation (EMR) [18, 19] have been developed, based on the concept of having a unified framework for modeling physical systems independently of their energetic domains [20].

In this paper, we focus on the dynamic modeling of nonlinear mechanical systems whose energy E_n can be expressed in the quadratic form $E_n(\mathbf{x}, \dot{\mathbf{x}}) = \frac{1}{2}\dot{\mathbf{x}}^T \mathbf{M}(\mathbf{x}) \dot{\mathbf{x}}$, where $\mathbf{M}(\mathbf{x})$ is a full rank symmetric matrix, while the terms $\mathbf{x} = [x_1, x_2, \dots, x_N]$ and $\dot{\mathbf{x}} = [\dot{x}_1, \dot{x}_2, \dots, \dot{x}_N]$ are the vector of the generalized coordinates and its time derivative, respectively. In this context, the typically used description of the system dynamic model is the so-called Euler-Lagrange form [11]:

$$\mathbf{M}(\mathbf{x}) \ddot{\mathbf{x}} + \mathbf{N}(\mathbf{x}, \dot{\mathbf{x}}) \dot{\mathbf{x}} = \boldsymbol{\tau} \quad \leftrightarrow \quad \mathbf{M} \ddot{\mathbf{x}} + \mathbf{N} \dot{\mathbf{x}} = \boldsymbol{\tau}, \quad (1)$$

where $\boldsymbol{\tau}$ is the generalized wrench vector. Hereinafter, the explicit dependencies “ (\mathbf{x}) ” and “ $(\mathbf{x}, \dot{\mathbf{x}})$ ” for matrices \mathbf{M} and \mathbf{N} , respectively, will be omitted for the sake of brevity.

In this paper, a new alternative formulation of the model (1) is proposed, which is called *factorized* form and is based on the calculation of the characterizing factorization matrix \mathbf{T} . Together with this new formulation, we also provide the steps of a modeling procedure allowing to systematically obtain the model equations, as well as the factorization matrix \mathbf{T} . The derivative-causality and integral-causality implementations of the factorized model are derived through rigorous theorems supported by analytical proofs.

Furthermore, the advantages of the new proposed factorized model are shown in terms of:

[✉]Corresponding author

Email addresses: davide.tebaldi@unimore.it (Davide Tebaldi[✉]), roberto.zanasi@unimore.it (Roberto Zanasi[✉])

- a) better simulation performances of the factorized model for time-varying physical systems, such as the FTV in Sec. 4, compared to the Euler-Lagrange formulation. For the FTV case study, it is shown that the simulation results given by the factorized model in the noisy scenario remain the same as the noiseless case.
- b) better simulation performances of the factorized model in terms of execution time when computing the inverse dynamics of a robotic manipulator compared to the Euler-Lagrange formulation.

The remainder of this paper is structured as follows. The proposed factorized model is given in Sec. 2, together with the proposed modeling procedure. The different case studies, showing the good performances of the proposed factorized model, are addressed in Sec. 3, Sec. 4 and Sec. 5, respectively. Finally, the appendix part is dedicated to analytical proof, and the conclusions are given in Sec. 6.

2. Proposed Model Formulation and Modeling Procedure

This section deals with the introduction of the proposed factorized model in Sec. 2.1, and with the introduction of the proposed modeling procedure allowing to compute the factorization matrix in Sec. 2.2.

2.1. Factorized Model Formulation

Theorem 1. *The Euler-Lagrange model (1) can be expressed in the following alternative factorized form:*

$$\mathbf{T}^T \frac{d}{dt} (\mathbf{T} \dot{\mathbf{x}}) = \boldsymbol{\tau}, \quad (2)$$

where the factorization matrix \mathbf{T} , which can also be rectangular with more rows than columns, is such that the matrices \mathbf{M} and \mathbf{N} in (1) can be expressed as follows:

$$\mathbf{M} = \mathbf{T}^T \mathbf{T}, \quad \mathbf{N} = \mathbf{T}^T \dot{\mathbf{T}}, \quad (3)$$

where $\dot{\mathbf{T}}$ is the time derivative of matrix \mathbf{T} . \square

Proof. The left side of model (2) can be written as:

$$\mathbf{T}^T \frac{d}{dt} (\mathbf{T} \dot{\mathbf{x}}) = \underbrace{\mathbf{T}^T \mathbf{T}}_{\mathbf{M}} \ddot{\mathbf{x}} + \underbrace{\mathbf{T}^T \dot{\mathbf{T}}}_{\mathbf{N}} \dot{\mathbf{x}} \quad (4)$$

resulting in the Euler-Lagrange form (1).

The factorization matrix \mathbf{T} can be obtained using the modeling procedure described in the next Sec. 2.2.

Systems (1) and (2) are written using a derivative causality. While, for what concerns systems (1), the integral causality implementation can be obtained through direct inversion, the following theorem applies to the factorized system (2).

Theorem 2. *The integral causality implementation of the factorized form (2) cannot be obtained through direct model inversion because, when matrix \mathbf{T} is rectangular, the dimension of*

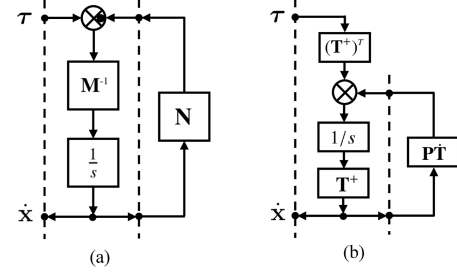


Figure 1: Power-oriented graph representation using integral causality of: (a) the Euler-Lagrange model (1), and (b) the factorized model (2).

vector $\mathbf{T} \dot{\mathbf{x}}$ in (2) is larger than that of vector $\dot{\mathbf{x}}$. Instead, the integral causality implementation of the factorized form (2) must be computed as follows:

$$\dot{\mathbf{x}} = \mathbf{T}^+ \int_0^t \left((\mathbf{T}^T)^T \boldsymbol{\tau} + \mathbf{P} \dot{\mathbf{T}} \dot{\mathbf{x}} \right) dt, \quad (5)$$

where $\mathbf{T}^+ = (\mathbf{T}^T \mathbf{T})^{-T} \mathbf{T}^T$ is the pseudo-inverse of matrix \mathbf{T} , and $\mathbf{P} = \mathbf{I} - \mathbf{T} \mathbf{T}^+$ is an orthogonal projection matrix on subspace $\text{Ker}(\mathbf{T}^T)$. \square

The proof of Theorem 2 is reported in App. A.

The Power-Oriented Graphs (POG) [17] representation of the integral implementations of the two models (1) and (2), which are suitable for direct implementation in the Simulink environment, are shown in Fig. 1. Specifically, Fig. 1(a) shows the power-oriented graph representation of the Euler-Lagrange model (1) in integral form, while Fig. 1(b) shows the power-oriented graph representation of the factorized model (2) in integral form.

2.2. Modeling Procedure

The dynamic equations of the considered class of mechanical systems can be systematically computed as follows:

- 1) Let n denote the number of coordinates variables x_i present in the system, for $i \in [1, 2, \dots, n]$, and let $\mathbf{x} = [x_1, x_2, \dots, x_n]^T$ denote the coordinates vector.
- 2) Let m denote the number of masses m_j in the system, for $j \in [1, 2, \dots, m]$, and let r_j denote the degrees of freedom in the space (translational and rotational) of mass m_j .
- 3) Write the position $P_{j,k}(\mathbf{x})$ of each degree of freedom k of each mass m_j , for $k \in [1, 2, \dots, r_j]$ and $j \in [1, 2, \dots, m]$. Let $\mathbf{P}_j(\mathbf{x}) = [P_{j,1}, P_{j,2}, \dots, P_{j,r_j}]^T$ denote the position vector of each mass m_j , and let $\mathbf{P}_0(\mathbf{x}) = [\mathbf{P}_1, \mathbf{P}_2, \dots, \mathbf{P}_m]^T$ denote the overall mass position vector of the system. At this point, other approaches in the literature would proceed in the direct writing of the differential equations characterizing the considered system [21]. In this paper, we introduce the factorized model formulation (2) instead, and we propose an automatic way of computing the factorization matrix \mathbf{T} characterizing it, through the subsequent steps.
- 4) Let $N_{j,k}$ denote the inertial coefficient (mass $m_{j,k}$ or inertial coefficient $J_{j,k}$) of each degree of freedom k of each mass m_j . Let $\mathbf{N}_j = [N_{j,1}, N_{j,2}, \dots, N_{j,r_j}]$ denote the inertial vector of

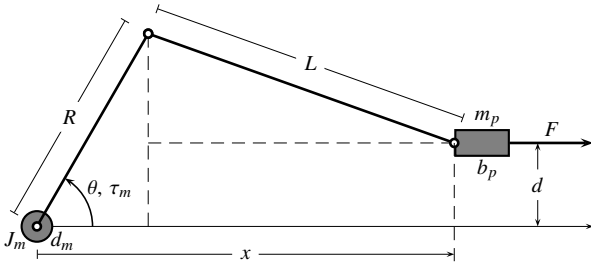


Figure 2: Structure of the crank-connecting rod system.

mass m_j , and let $\mathbf{N}_0 = \text{diag}([\mathbf{N}_j, \mathbf{N}_j, \dots, \mathbf{N}_j])$ denote a diagonal matrix of all the inertial coefficients of the system.

5) The matrix \mathbf{T} of the factorized model (2) can be computed as follows:

$$\mathbf{T} = \sqrt{\mathbf{N}_0} \mathbf{H}_0, \quad \text{where} \quad \mathbf{H}_0 = \frac{\partial \mathbf{P}_0(\mathbf{x})}{\partial \mathbf{x}}. \quad (6)$$

The system matrices \mathbf{M} and \mathbf{N} of the Euler-Lagrange model (1) can be obtained using (3).

3. Dynamic Model of a crank-connecting rod system

Reference is made to the crank-connecting rod system shown in Fig. 2 as a first case study, composed of two masses. Applying the procedure of Sec. 2.2, in this case the system coordinate variable x is the angular position $x = \theta$ shown in Fig. 2, and the generalized torque τ is $\tau = -d_m - H^2(\theta)b_p + \tau_m + H(\theta)F$, where $H(\theta)$ is defined in (8). Each mass is characterized by one degree of freedom, see step 2) of the modeling procedure. The position vectors of the two masses at step 3) are the following:

$$\mathbf{P}_1 = \theta, \quad \mathbf{P}_2 = R \cos(\theta) + \sqrt{L^2 - (R \sin(\theta) - d)^2}.$$

The vector \mathbf{P}_0 and the matrix \mathbf{N}_0 have the following structure:

$$\mathbf{P}_0 = \begin{bmatrix} \mathbf{P}_1 \\ \mathbf{P}_2 \end{bmatrix}, \quad \mathbf{N}_0 = \begin{bmatrix} J_m & 0 \\ 0 & m_p \end{bmatrix},$$

while the vectors \mathbf{H}_0 and the factorization matrix \mathbf{T} are given by:

$$\mathbf{H}_0 = \frac{\partial \mathbf{P}_0}{\partial \theta} = \begin{bmatrix} 1 \\ H(\theta) \end{bmatrix}, \quad \mathbf{T} = \sqrt{\mathbf{N}_0} \mathbf{H}_0 = \begin{bmatrix} \sqrt{J_m} \\ \sqrt{m_p} H(\theta) \end{bmatrix}, \quad (7)$$

where

$$H(\theta) = \frac{\partial \mathbf{P}_2}{\partial \theta} = -R \sin \theta + \frac{R \cos \theta (d - R \sin \theta)}{\sqrt{L^2 - (R \sin \theta - d)^2}}. \quad (8)$$

The matrix \mathbf{T} in (7) fully defines the proposed factorized model (2). Additionally, using (3) and (7), the matrices \mathbf{M} and \mathbf{N} of the Euler-Lagrange model (1) can be obtained as follows:

$$\mathbf{M}(\theta) = \mathbf{T}^T \mathbf{T} = M(\theta) = J_m + m_p H^2(\theta),$$

$$\mathbf{N}(\theta, \dot{\theta}) = \mathbf{T}^T \dot{\mathbf{T}} = \frac{\dot{M}(\theta)}{2} = m_p H(\theta) \dot{H}(\theta).$$

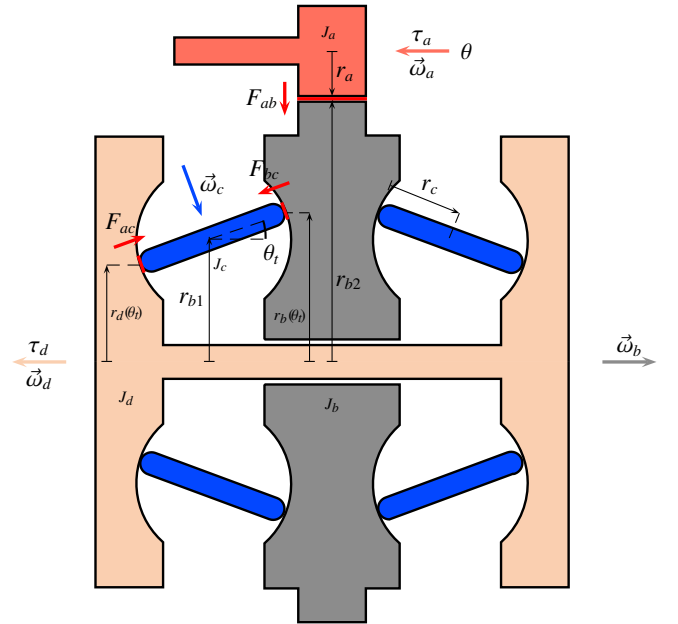


Figure 3: Schematic representation of the Full Toroidal Variator.

4. Dynamic Model of a Full Toroidal Variator

The Full Toroidal Variator (FTV) is a key element in automotive, that finds applications such as Kinetic Energy Recovery System (KERS) and Infinitely Variable Transmission (IVT). A schematic of the considered FTV is shown in Fig. 3 [4], where the speed-ratio is a function of the rollers tilt angle $\theta_t = \theta_t(t)$. In this case, the system is composed by four rotating masses, and the generalized torque τ is $\tau = -(b_a + R_1^2 b_b + R_2^2(\theta_t) b_c + R_3^2(\theta_t) b_d) \omega_a + \tau_a$, where R_1 , $R_2(\theta_t)$ and $R_3(\theta_t)$ are defined in (9). The configuration variable x at step 1) of the procedure proposed in Sec. 2.2 is the angular position $x = \theta_a = \theta$ of inertia J_a . Each mass is characterized by one degree of freedom, see step 2) of the modeling procedure. The position vector \mathbf{P}_0 of the system at step 3) is given by:

$$\mathbf{P}_0 = \begin{bmatrix} \mathbf{P}_a \\ \mathbf{P}_b \\ \mathbf{P}_c \\ \mathbf{P}_d \end{bmatrix} = \begin{bmatrix} \theta_a \\ \theta_b \\ \theta_c \\ \theta_d \end{bmatrix} = \begin{bmatrix} \theta \\ \frac{r_a}{r_{b2}} \theta_a \\ \frac{r_b(\theta_t)}{r_c} \theta_b \\ \frac{r_c}{r_d(\theta_t)} \theta_c \end{bmatrix} = \begin{bmatrix} 1 \\ R_1 \\ R_2(\theta_t) \\ R_3(\theta_t) \end{bmatrix} \theta = \mathbf{R}(\theta_t) \theta,$$

where the gear ratios R_1 , $R_2(\theta_t)$ and $R_3(\theta_t)$ are defined as:

$$R_1 = \frac{r_a}{r_{b2}}, \quad R_2(\theta_t) = \frac{r_a r_b(\theta_t)}{r_{b2} r_c}, \quad R_3(\theta_t) = \frac{r_a r_b(\theta_t)}{r_{b2} r_d(\theta_t)}, \quad (9)$$

and the radii $r_b(\theta_t)$ and $r_d(\theta_t)$ are given by:

$$r_b(\theta_t) = (r_{b1} + r_c \sin \theta_t), \quad r_d(\theta_t) = (r_{b1} - r_c \sin \theta_t).$$

The matrix \mathbf{N}_0 is $\mathbf{N}_0 = \text{diag}([J_a, J_b, J_c, J_d])$, while the vectors \mathbf{H}_0 and the factorization matrix \mathbf{T} have the following structure:

$$\mathbf{H}_0 = \frac{\partial \mathbf{P}_0}{\partial \theta} = \mathbf{R}(\theta_t), \quad \mathbf{T} = \sqrt{\mathbf{N}_0} \mathbf{H}_0 = \sqrt{\mathbf{N}_0} \mathbf{R}(\theta_t). \quad (10)$$

Table 1: Parameters of the Full Toroidal Variator.

| |
|---|
| $J_a = 0.026, J_b = 7.56 \cdot 10^{-4}, J_c = 0.0018, J_d = 0.179 \text{ kg m}^2$ |
| $r_a = 17.2, r_b = 51.5, r_c = 27.5, r_d = 34.3 \text{ mm}$ |

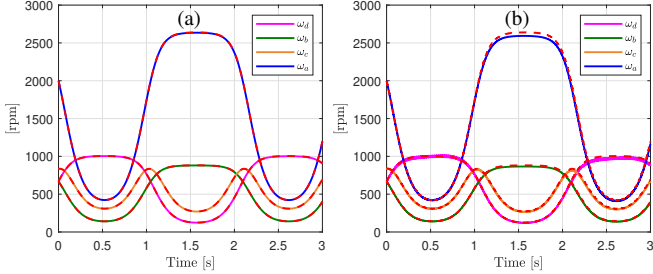


Figure 4: Full Toroidal Variator: Simulation results in the noiseless scenario (a) and noisy scenario (b). The colored results are given by the Euler-Lagrange model, while the red dashed results are given by the proposed factorized model.

The matrix \mathbf{T} in (10) fully defines the proposed factorized model (2). Using (3) and (10), the matrices \mathbf{M} and \mathbf{N} of the Euler-Lagrange model (1) can also be obtained as follows:

$$\begin{aligned} \mathbf{M}(\theta_t) &= \mathbf{T}^T \mathbf{T} = M(\theta_t) = J_a + J_b R_1^2 + J_c R_2^2(\theta_t) + J_d R_3^2(\theta_t), \\ \mathbf{N}(\theta_t, \dot{\theta}_t) &= \mathbf{T}^T \dot{\mathbf{T}} = \frac{\dot{M}(\theta_t)}{2} = r_b(\theta_t) r_c \dot{\theta}_t \cos \theta_t R_1^2 \left(\frac{J_c}{r_c^2} + \frac{2r_{b1}J_d}{r_d^3(\theta_t)} \right). \end{aligned} \quad (11)$$

Remark 1. Matrix $\mathbf{N}(\theta_t, \dot{\theta}_t)$ in (11), present in the Euler-Lagrange model, is function of both θ_t and $\dot{\theta}_t$, where $\dot{\theta}_t$ is not an internal system variable and therefore must be computed numerically from the available measurements of the external variable θ_t representing the rollers tilt angle. This makes the Euler-Lagrange model sensitive to measurement noise, as further discussed in the results presented in Sec. 4.1. The aforementioned drawback is not present in the proposed factorized model (2), because it does not depend on variable $\dot{\theta}_t$.

4.1. Simulation of the Full Toroidal Variator system

The results given by the simulation of the FTV using the Euler-Lagrange model (1) and the factorized model (2) have been compared in the following two conditions: 1) noiseless scenario; 2) noisy scenario. The frictionless case and the parameters in Table 1 have been considered. The input torques have been assumed equal to zero, the initial condition is $\omega_{a0} = 2000 \text{ rpm}$, and the tilt angle is $\theta_t = 1.22 \sin(3t)$. In the noisy case, a disturbance $d = 12.2 \cdot 10^{-3} \sin(3 \cdot 10^3 t)$ has been superimposed to the tilt angle θ_t . The results are shown in Fig. 4. It can be noticed that both the Euler-Lagrange model and the factorized model give the same results in the noiseless scenario. Conversely, in the noisy scenario, the proposed factorized model yields the same results as in the noiseless scenario, thanks to its independence from $\dot{\theta}_t$, whereas the performance of the Euler-Lagrange model degrades. In fact, the maximum and mean percentage differences $\max(|\Delta_\omega|)$ and $\text{mean}(|\Delta_\omega|)$ of the angular velocities given by the Euler-Lagrange model with respect to the correct ones (given by the proposed factorized

Table 2: Mean and maximum percentage differences of the angular velocities given by the Euler-Lagrange model, with respect to those given by the proposed factorized model, in the noisy scenario.

| | ω_a | ω_b | ω_c | ω_d |
|-------------------------------|------------|------------|------------|------------|
| mean($ \Delta_\omega $) [%] | 1.73 | 1.73 | 1.74 | 1.81 |
| max($ \Delta_\omega $) [%] | 2.35 | 2.35 | 3.60 | 5.02 |

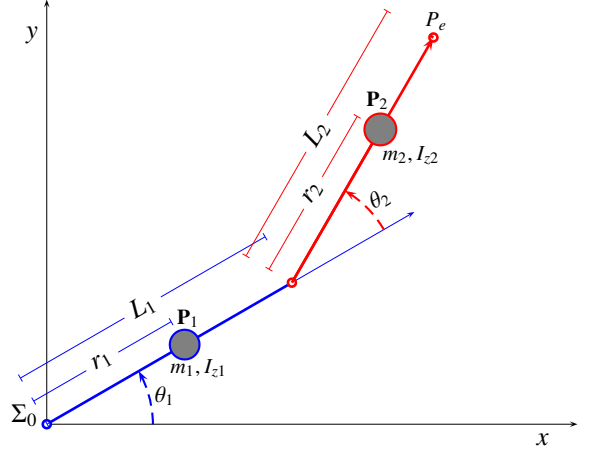


Figure 5: Planar robot with 2-DoF expressed in the fixed frame Σ_0 .

model) are shown in Table 2, showing a non-negligible degradation of the Euler-Lagrange model results even with the considered small disturbance d .

5. Dynamic Model of a Planar robot with 2 DoF

Reference is made to the planar robot with 2 DoF shown in Fig. 5, expressed in the fixed frame Σ_0 . Applying the modeling approach proposed in Sec. 2.2, the planar positions \mathbf{P}_1 and \mathbf{P}_2 of the two masses m_1 and m_2 are the following:

$$\mathbf{P}_1 = \theta_1, \quad \mathbf{P}_2 = \begin{bmatrix} L_1 \cos(\theta_1) + r_2 \cos(\theta_1 + \theta_2) \\ L_1 \sin(\theta_1) + r_2 \sin(\theta_1 + \theta_2) \\ \theta_1 + \theta_2 \end{bmatrix}. \quad (12)$$

The vectors \mathbf{x} , \mathbf{P}_0 and the matrix $\mathbf{H}_0(\mathbf{x})$ are given by:

$$\mathbf{x} = \begin{bmatrix} x_1 \\ x_2 \end{bmatrix} = \begin{bmatrix} \theta_1 \\ \theta_2 \end{bmatrix}, \quad \mathbf{P}_0 = \begin{bmatrix} \mathbf{P}_1 \\ \mathbf{P}_2 \end{bmatrix}, \quad \mathbf{H}_0(\mathbf{x}) = \frac{\partial \mathbf{P}_0}{\partial \mathbf{x}} = \begin{bmatrix} \frac{\partial \mathbf{P}_0}{\partial \theta_1} & \frac{\partial \mathbf{P}_0}{\partial \theta_2} \end{bmatrix}.$$

The diagonal matrix \mathbf{N}_0 has the following structure:

$$\mathbf{N}_0 = \text{diag}\{[m_1 r_1^2 + I_{z1}, m_2, m_2, I_{z2}]\},$$

while the matrix \mathbf{T} characterizing the proposed factorized model (2) can be computed as $\mathbf{T} = \sqrt{\mathbf{N}_0} \mathbf{H}_0$. The matrices of the Euler-Lagrange model (1) can be computed using (3). Specifically, matrix \mathbf{M} has the following structure:

$$\mathbf{M}(\mathbf{x}) = \mathbf{T}^T \mathbf{T} = \begin{bmatrix} \alpha + 2\beta \cos \theta_2 & \delta + \beta \cos \theta_2 \\ \delta + \beta \cos \theta_2 & \delta \end{bmatrix}, \quad (13)$$

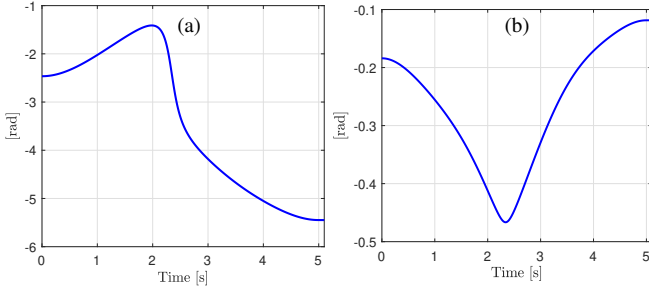


Figure 6: Considered trajectory for the 2-DoF planar robot: (a) θ_1 and (b) θ_2 .

where the parameters α , β and δ are defined as follows:

$$\alpha = I_{z1} + m_1 r_1^2 + m_2 L_1^2 + I_{z2} + m_2 r_2^2, \\ \beta = m_2 L_1 r_2, \quad \delta = I_{z2} + m_2 r_2^2.$$

Finally, matrix \mathbf{N} has the following structure:

$$\mathbf{N}(\mathbf{x}, \dot{\mathbf{x}}) = \mathbf{T}^T \dot{\mathbf{T}} = \begin{bmatrix} -\beta \sin \theta_2 \dot{\theta}_2 & -\beta \sin \theta_2 (\dot{\theta}_1 + \dot{\theta}_2) \\ \beta \sin \theta_2 \dot{\theta}_1 & 0 \end{bmatrix}.$$

5.1. Simulation of the Planar Robot With 2 DOF

Many applications require robots to be controlled using inverse dynamics control [11]. The latter approach necessarily requires to compute the inverse dynamics of the manipulator. Assuming friction and gravity terms to be already compensated for, the inverse dynamics of robotic systems is typically expressed using the Euler-Lagrange model (1) [11]:

$$\boldsymbol{\tau} = \mathbf{B}(\mathbf{x}) \ddot{\mathbf{x}} + \mathbf{C}(\mathbf{x}, \dot{\mathbf{x}}) \dot{\mathbf{x}} = \mathbf{M} \ddot{\mathbf{x}} + \mathbf{N} \dot{\mathbf{x}}, \quad (14)$$

where $\dot{\mathbf{x}}$ is the state vector, $\mathbf{M} = \mathbf{B}(\mathbf{x})$ is the inertia matrix, and $\mathbf{N} = \mathbf{C}(\mathbf{x}, \dot{\mathbf{x}})$ is the Coriolis forces matrix. In this section, we compare the Euler-Lagrange model (14) and the proposed factorized model (2) in computing the inverse dynamics of the considered 2-DoF planar robot in [22] when the desired joint space trajectory $\mathbf{x} = [\theta_1 \ \theta_2]^T$ is the one shown in Fig. 6. The two models have been implemented in the Simulink environment, using MATLAB R2023b, and simulated in automatic solver selection mode in order to let MATLAB choose the best solver for each simulation, by using the same solver details. The results in terms of torque vector $\boldsymbol{\tau} = [\tau_1 \ \tau_2]^T$ are very close, as shown in Table 3 by the maximum and mean percentage differences $\max(|\Delta\tau_1|)$, $\text{mean}(|\Delta\tau_1|)$, $\max(|\Delta\tau_2|)$ and $\text{mean}(|\Delta\tau_2|)$ between the torque profiles τ_1 and τ_2 generated by the two models. At the same time, Fig. 7 shows the lower execution time (computed for 100 executions) given by the factorized model compared to the Euler-Lagrange model. The average reduction in the execution time given by the factorized model is 17.08 % compared to the Euler-Lagrange model, showing the better performances of the factorized model over the Euler-Lagrange one.

6. Conclusions

This paper has addressed the proposal of a new formulation for the dynamic model of nonlinear mechanical systems - called

Table 3: Mean and maximum percentage differences between the torque profiles τ_1 and τ_2 generated by the two model formulations: Euler-Lagrange model and the proposed factorized model.

| mean($ \Delta\tau_1 $) [%] | max($ \Delta\tau_1 $) [%] | mean($ \Delta\tau_2 $) [%] | max($ \Delta\tau_2 $) [%] |
|------------------------------|-----------------------------|------------------------------|-----------------------------|
| 0.071 | 0.016 | 0.32 | 0.32 |

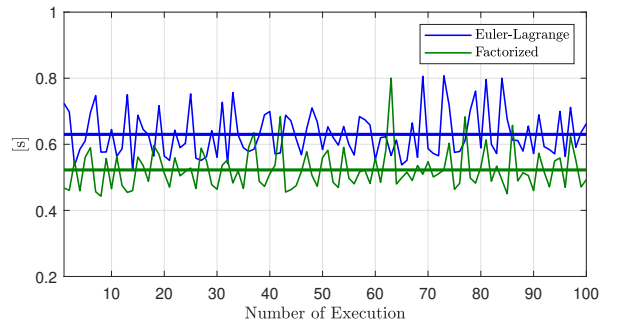


Figure 7: Execution time of the Euler-Lagrange model and of the factorized model in computing the inverse dynamics over 100 executions. The horizontal lines represent the average execution times. The average reduction in the execution time given by the factorized model is 17.08 % compared to the Euler-Lagrange model.

factorized model formulation - as well as the proposal of modeling approach enabling the user to automatically derive the system model. The proposed factorized model can be applied to different physical system case studies, and has been shown to give superior performance when compared with the Euler-Lagrange model in terms of: robustness against measurement noise for physical systems where the system matrices exhibit a dependence on some external variables, and in terms of execution time when computing the inverse dynamics of the system.

Funding

The work was partly supported by the University of Modena and Reggio Emilia through the action FARD (Finanziamento Ateneo Ricerca Dipartimentale) 2023-2024, and funded under the National Recovery and Resilience Plan (NRRP), Mission 04 Component 2 Investment 1.5 - NextGenerationEU, Call for tender n. 3277 dated 30/12/2021 Award Number: 0001052 dated 23/06/2022.

Appendix A: Proof of Theorem 2.

Let \mathbf{T}^+ denote the Moore-Penrose pseudo-inverse of matrix \mathbf{T} . If matrix \mathbf{T} in (3) is square, then $\mathbf{T}^+ = \mathbf{T}^{-1}$. If \mathbf{T} is rectangular, then it surely has more rows than columns since \mathbf{M} is full rank, and thus $\mathbf{T}^+ = (\mathbf{T}^T \mathbf{T})^{-1} \mathbf{T}^T$. Matrix $\mathbf{T} \mathbf{T}^+ = \mathbf{T} (\mathbf{T}^T \mathbf{T})^{-1} \mathbf{T}^T$ is an orthogonal projection matrix on subspace $\text{Im}(\mathbf{T})$, and as such it is symmetric:

$$\mathbf{T} \mathbf{T}^+ = \mathbf{T} (\mathbf{T}^T \mathbf{T})^{-1} \mathbf{T}^T = (\mathbf{T} (\mathbf{T}^T \mathbf{T})^{-1} \mathbf{T}^T)^T = (\mathbf{T} \mathbf{T}^+)^T. \quad (\text{A.1})$$

Using (A.1), Eq. (2) can be rewritten as follows:

$$\begin{aligned} (\mathbf{T}^+)^T \mathbf{T}^T \frac{d}{dt} (\mathbf{T} \dot{\mathbf{x}}) &= (\mathbf{T}^+)^T \boldsymbol{\tau} \\ (\mathbf{T} \mathbf{T}^+)^T \frac{d}{dt} (\mathbf{T} \dot{\mathbf{x}}) &= (\mathbf{T}^+)^T \boldsymbol{\tau} \\ (\mathbf{T} \mathbf{T}^+)^T \frac{d}{dt} (\mathbf{T} \dot{\mathbf{x}}) &= (\mathbf{T}^+)^T \boldsymbol{\tau}. \end{aligned} \quad (\text{A.2})$$

Let $\mathbf{P} = (\mathbf{I} - \mathbf{T}\mathbf{T}^+)$ denote the orthogonal projection matrix on subspace $\text{Ker}(\mathbf{T}^+)$. Using \mathbf{P} , the following equalities can be obtained from (A.2):

$$\begin{aligned} (\mathbf{T}\mathbf{T}^+) \frac{d}{dt}(\mathbf{T}\dot{\mathbf{x}}) &= (\mathbf{T}^+)^T \boldsymbol{\tau} \\ (\mathbf{I} - \mathbf{P}) \frac{d}{dt}(\mathbf{T}\dot{\mathbf{x}}) &= (\mathbf{T}^+)^T \boldsymbol{\tau} \\ \frac{d}{dt}(\mathbf{T}\dot{\mathbf{x}}) &= \mathbf{P} \frac{d}{dt}(\mathbf{T}\dot{\mathbf{x}}) + (\mathbf{T}^+)^T \boldsymbol{\tau} \quad (\text{A.3}) \\ \frac{d}{dt}(\mathbf{T}\dot{\mathbf{x}}) &= \mathbf{P}(\dot{\mathbf{T}}\dot{\mathbf{x}} + \mathbf{T}\ddot{\mathbf{x}}) + (\mathbf{T}^+)^T \boldsymbol{\tau} \\ \frac{d}{dt}(\mathbf{T}\dot{\mathbf{x}}) &= \mathbf{P}\dot{\mathbf{T}}\dot{\mathbf{x}} + (\mathbf{T}^+)^T \boldsymbol{\tau}, \end{aligned}$$

where the latter equality holds because $\mathbf{T}\dot{\mathbf{x}} \in \text{Im}(\mathbf{T})$. Integrating both sides of the last equality in (A.3) and left-multiplying by matrix \mathbf{T}^+ yield Eq. (5).

References

- [1] J. C. Maxwell, On physical lines of force, *Philosophical Magazine* 21 (139) (1861) 161–175.
- [2] H. N. Z. Matin, Y. Yeo, X. Gong, M. L. D. Monache, On the analytical properties of a nonlinear microscopic dynamical model for connected and automated vehicles, *IEEE Control Systems Letters* 8 (2024) 1607–1612.
- [3] J. Lagrange, *Mécanique analytique*, no. v. 1 in *Mécanique analytique*, Ve Courcier, 1811.
- [4] D. Tebaldi, R. Zanasi, Systematic modeling of complex time-variant gear systems using a power-oriented approach, *Control Engineering Practice* 132 (2023) 105420.
- [5] H. Zhang, M. Dou, J. Deng, Loss-minimization strategy of nonsinusoidal back emf pmsm in multiple synchronous reference frames, *IEEE Transactions on Power Electronics* 35 (8) (2020) 8335–8346.
- [6] D. D. C., R. K. P., An adaptive continuous nonsingular fast terminal smc for permanent magnet synchronous motor fed electric vehicle, *European Journal of Control* 75 (2024) 100931.
- [7] W. Lhomme, A. Bouscayrol, S. A. Syed, S. Roy, F. Gailly, O. Pape, Energy savings of a hybrid truck using a ravigneaux gear train, *IEEE Transactions on Vehicular Technology* 66 (10) (2017) 8682–8692.
- [8] A. Tilli, A. Bosso, C. Conficoni, Towards sensorless observers for sinusoidal electric machines with variable speed and no mechanical model: A promising approach for pmsms, *Systems & Control Letters* 123 (2019) 16–23.
- [9] R. Fuchs, Y. Hasuda, I. James, Full toroidal ivt variator dynamics, 2002.
- [10] F. Zhang, L. Wang, S. Coskun, H. Pang, Y. Cui, J. Xi, Energy management strategies for hybrid electric vehicles: Review, classification, comparison, and outlook, *Energies* 13 (13) (2020).
- [11] B. Siciliano, L. Sciavicco, L. Villani, G. Oriolo, *Robotics: Modelling, Planning and Control*, 1st Edition, Springer Publishing Company, Incorporated, 2008.
- [12] T. Tsumugiwa, Y. Fuchikami, A. Kamiyoshi, R. Yokogawa, K. Yoshida, Stability analysis for impedance control of robot in human-robot cooperative task system, *Journal of Advanced Mechanical Design, Systems, and Manufacturing* 1 (1) (2007) 113–121.
- [13] D. Sirintuna, T. Kastritsi, I. Ozdamar, J. M. Gandarias, A. Ajoudani, Enhancing human–robot collaborative transportation through obstacle-aware vibrotactile warning and virtual fixtures, *Robotics and Autonomous Systems* 178 (2024) 104725.
- [14] R. V. Polyuga, A. J. van der Schaft, Effort- and flow-constraint reduction methods for structure preserving model reduction of port-hamiltonian systems, *Systems & Control Letters* 61 (3) (2012) 412–421.
- [15] R. Loureiro, R. Merzouki, B. O. Bouamama, Bond graph model based on structural diagnosability and recoverability analysis: Application to intelligent autonomous vehicles, *IEEE Transactions on Vehicular Technology* 61 (3) (2012) 986–997.
- [16] J. Gonzalez, C. Sueur, Unknown input observer with stability: A structural analysis approach in bond graph, *European Journal of Control* 41 (2018) 25–43.
- [17] D. Tebaldi, R. Zanasi, The power-oriented graphs modeling technique: From the fundamental principles to the systematic, step-by-step modeling of complex physical systems, *IEEE Access* 13 (2025) 32470–32485.
- [18] K. Li, W. Lhomme, A. Bouscayrol, A state of charge planning method of a plug-in hybrid electric truck with readily available navigation signals, *IEEE Transactions on Vehicular Technology* 73 (5) (2024) 6093–6105.
- [19] A. Bouscayrol, B. Davat, B. de Fornel, B. Francois, J. P. Hautier, F. Meibody-Tabar, M. Pietrzak-David, Multi-converter multi-machine systems: application for electromechanical drives, *The European Physical Journal - Applied Physics* 10 (2) (2000) 131–147. doi:10.1051/epjap:2000124.
- [20] G. Kron, *Tensor analysis of networks*, J. Wiley & Sons New York, 1939.
- [21] D. C. Karnopp, D. L. Margolis, R. C. Rosenberg, Modeling, simulation, and control of mechatronic systems, in: *System Dynamics*, 2012.
- [22] Mathworks, Ltv model of two-link robot, <https://it.mathworks.com/help/control/ug/linear-time-varying-robot-model.html>, accessed: 2026-01-02.